Biol Trace Elem Res (2014) 159:379–392
DOI 10.1007/s12011-014-9964-0

Water-Soluble Ruthenium Complexes Bearing Activity Against Protozoan Parasites

Cynthia Sarniguet · Jeannette Toloza · Micaella Cipriani · Michel Lapier · Marisol Vieites · Yanis Toledano-Magaña · Juan Carlos García-Ramos · Lena Ruiz-Azuara · Virtudes Moreno · Juan Diego Maya · Claudio Olea Azar · Dinorah Gambino · Lucía Otero

Received: 23 February 2014 / Accepted: 31 March 2014 / Published online: 17 April 2014

Abstract Parasitic illnesses are major causes of human disease and misery worldwide. Among them, both amebiasis and Chagas disease, caused by the protozoan parasites, *Entamoeba histolytica* and *Trypanosoma cruzi*, are responsible for thousands of annual deaths. The lack of safe and effective chemotherapy and/or the appearance of current drug resistance make the development of novel pharmacological tools for their treatment relevant. In this sense, within the framework of the medicinal inorganic chemistry, metal-based drugs appear to be a good alternative to find a pharmacological answer to parasitic diseases. In this work, novel ruthenium complexes $[RuCl_2(HL)(HPTA)_2]Cl_2$ with HL = bioactive 5-nitrofuryl containing thiosemicarbazones and PTA= 1,3,5-triaza-7-phosphaadamantane have been synthesized and fully characterized. PTA was included as co-ligand in order to modulate complexes aqueous solubility. In fact, obtained complexes were water soluble. Their activity against *T. cruzi* and *E. histolytica* was evaluated in vitro. $[RuCl_2(HL4)(HPTA)_2]Cl_2$ complex, with HL4= *N*-phenyl-5-nitrofuryl-thiosemicarbazone, was the most active compound against both parasites. In particular, it showed an excellent activity against *E. histolytica* (half maximal inhibitory concentration (IC_{50})=5.2 μM), even higher than that of the reference drug metronidazole. In addition, this complex turns out to be selective for *E. histolytica* (selectivity index (SI) >38). The potential mechanism of antiparasitic action of the obtained ruthenium complexes could involve oxidative stress for both parasites. Additionally, complexes could interact with DNA as second potential target by an intercalative-like mode. Obtained results could be considered a contribution in the search for metal compounds that could be active against multiple parasites.

Electronic supplementary material The online version of this article (doi:10.1007/s12011-014-9964-0) contains supplementary material, which is available to authorized users.

C. Sarniguet · M. Cipriani · M. Vieites · D. Gambino (✉) · L. Otero (✉)
Cátedra de Química Inorgánica, DEC, Facultad de Química, Universidad de la República, Gral. Flores 2124, C. C. 1157, 11800 Montevideo, Uruguay
e-mail: dgambino@fq.edu.uy
e-mail: luotero@fq.edu.uy

J. Toloza · C. O. Azar
Departamento de Química Inorgánica y Analítica, Facultad de Ciencias Químicas y Farmacéuticas, Universidad de Chile, Sergio Livingstone 1007, Casilla 233, Santiago, Chile

M. Lapier · J. D. Maya
Departamento de Farmacología Clínica y Molecular, ICBM, Facultad de Medicina, Universidad de Chile, Independencia 1027, Santiago, Chile

Y. Toledano-Magaña
Departamento de Inmunología, Instituto de Investigaciones Biomédicas, Universidad Nacional Autónoma de México, Avenida Universidad 3000, 04510 Mexico City, Mexico

J. C. García-Ramos · L. Ruiz-Azuara
Departamento de Química Inorgánica y Nuclear, Facultad de Química, Universidad Nacional Autónoma de México, Avenida Universidad 3000, 04510 Mexico, DF, Mexico

V. Moreno
Departamento de Química Inorgánica, Universitat Barcelona, Martí i Franquès 1-11, 08028 Barcelona, Spain

Keywords *Trypanosoma cruzi* · *Entamoeba histolytica* · Ruthenium · 5-Nitrofuryl containing thiosemicarbazones · PTA (1,3,5-triaza-7-phosphaadamantane)

Introduction

Amebiasis and Chagas disease, caused by the protozoan parasites *Entamoeba histolytica* (*E. histolytica*) and *Trypanosoma cruzi* (*T. cruzi*), respectively, are responsible for several human diseases, and they lead to thousands of annual deaths [1–3].

Chagas disease is a chronic, systemic, parasitic infection that affects about 8 million people in Latin America but also, due to immigration, hundreds of thousands in USA and Europe. Amebiasis is a health risk in almost all countries principally due to poor hygiene practices, resulting in 40,000 annual deaths [3–7].

Despite these illnesses that present high prevalence worldwide, treatment for Chagas disease and amebiasis is limited to a few drugs in the market (nifurtimox and benznidazole for the former and metronidazole for the latter), most of which are of low efficacy, show toxic side effects, and frequently lead to the appearance of resistant strains. The development of more efficient and safe drugs is still a challenge [8–12].

Metal-based drugs appear to be a good alternative to find a pharmacological answer to parasitic diseases. In particular, the complexation of transition metals with a proved or potential biologically active ligand could lead to enhance its pharmacological and chemical properties such as potency, toxicity, solubility, chemical stability, and lipophilicity. In addition, a metal-drug synergism could be achieved through a dual or multiple mechanism of action [12–19]. Some bioactive ligands that have been extensively explored in this sense are thiosemicarbazones. These small and versatile molecules have been related to many pharmacological activities, like antiparasitic, due to the highlighting results obtained against both *E. histolytica* and *T. cruzi*, among other parasites [12, 20–22].

In this frame, some of us have been involved in the development of metal complexes with antichagasic 5-nitrofuryl containing thiosemicarbazones (Fig. 1). We have rationally designed and developed more than fifty compounds including palladium, platinum, and ruthenium complexes as well as ruthenium organometallic compounds in order to evaluate the effect of metal complexation and the presence of different co-ligands on the pharmacological profile of the bioactive ligands. Most complexes resulted more or at least equally active than the corresponding ligands, and the activity could be correlated to properties like solubility, stability, lipophilicity, or protein interaction. Compound mechanisms of anti-*T. cruzi* action were also extensively studied [18, 23–32]. In addition, palladium, copper, vanadium, and ruthenium thiosemicarbazone complexes have been explored in order to obtain safer and more active drugs against *E. histolytica*. Most of the obtained compounds were more active than the corresponding ligands, showing promising amebicidal activity [12].

Based on these previous results, in this work, we have developed a new series of ruthenium complexes with the 5-nitrofuryl containing thiosemicarbazones shown in Fig. 1 as bioactive ligands. PTA (1,3,5-triaza-7-phosphaadamantane, Fig. 1) was included in the ruthenium coordination sphere in order to modulate water solubility of the compounds. PTA is a hydrophilic phosphine that has been extensively used as ligand in aqueous homogeneous catalysis [33, 34]. Recently, the interest in this ligand has been renewed due to its usefulness as ancillary ligand for medicinal chemistry purposes, as it is known to endow metal complexes with aqueous solubility and solubility in polar organic solvents [33, 34]. Ruthenium has been selected as metal center due to its suitable chemical and biological properties, i.e., biologically attainable oxidation states (II, III), coordination versatility, and octahedral geometry, that allow ancillary ligands, appropriate ligand substitution kinetics, low toxicity to humans related to metabolic similarities with iron [18, 35]. Finally, related to the potential mechanism of antiparasitic action of the ruthenium-PTA-thiosemicarbazone complexes, a dual mechanism of action could be expected, combining the pharmacological properties of the ligands and the metal. On one side, the main mode of action of the 5-nitrofuryl containing thiosemicarbazone compounds is related to the intracellular reduction of the nitro moiety followed by redox cycling, yielding reduced reactive oxygen species (ROS) that cause cellular damage [36]. On the other, one of the reported targets of ruthenium bioactive compounds is DNA [35]. Therefore, in addition to the synthesis, characterization, and evaluation of the activity against *E. histolytica* and *T. cruzi* of the complexes, their ability of generating intraparasitic oxidative stress as well as of interacting with DNA was studied.

Materials and Methods

All common laboratory chemicals were purchased from commercial sources and used without further purification. PTA (1,3,5-triaza-7-phosphaadamantane) was purchased from Sigma-Aldrich. $[RuCl_2(DMSO)_4]$, with dimethylsulfoxide (DMSO), was prepared according to literature procedures [37]. All 5-nitrofuryl containing thiosemicarbazones were synthesized using the previously reported methodology [36].

Syntheses of $[Ru^{II}Cl_2(HL)(HPTA)_2]Cl_2{\cdot}H_2O{\cdot}C_2H_5OH$

$[RuCl_2(DMSO)_4]$ (100 mg, 0.2 mmol) and PTA (65 mg, 0.4 mmol) were dissolved in 10 mL ethanol. The mixture was refluxed for 2 h after which the corresponding

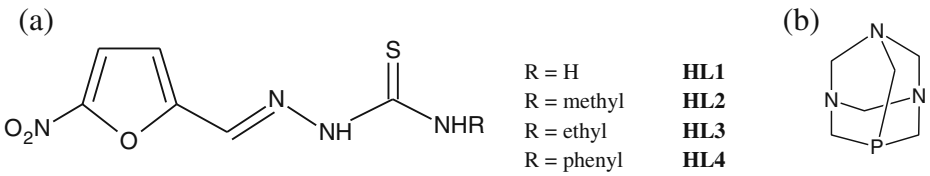

Fig. 1 **a** 5-nitrofuryl containing thiosemicarbazones. **b** PTA (1,3,5-triaza-7-phosphaadamantane)

thiosemicarbazone ligand HL (0.2 mmol) was added to the red solution. The solution was heated under reflux for 24 more hours. The obtained brown microcrystalline solid was filtered off and washed with ethanol (Scheme 1).

$[Ru^{II}Cl_2(HL1)(HPTA)_2]Cl_2{\cdot}H_2O{\cdot}C_2H_5OH$. Yield 92 mg, 54 %. Found C, 28.8; H, 4.6; N, 16.6; S, 4.0; H_2O + C_2H_5OH 7.8 %. Calc. for $C_{20}H_{40}N_{10}O_5SP_2Cl_4Ru$ C, 28.7; H, 4.8; N, 16.7; S, 3.8; H_2O + C_2H_5OH 7,6 %. $^{31}P\{^1H\}$ NMR (121.4 MHz, D_2O) δ = −11.40 (s, 1P, HPTA), −12.58 (s, 1P, HPTA).

$[Ru^{II}Cl_2(HL2)(HPTA)_2]Cl_2{\cdot}H_2O{\cdot}C_2H_5OH$. Yield 83 mg, 48 %. Found C, 29.7; H, 4.9; N, 16.6; S, 3.8; H_2O + C_2H_5OH 7.2 %. Calc. for $C_{21}H_{42}N_{10}O_5SP_2Cl_4Ru$ C, 29.6; H, 4.9; N, 16.4; S, 3.8; H_2O + C_2H_5OH 7.5 %. $^{31}P\{^1H\}$ NMR (121.4 MHz, D_2O) δ = −11.51 (s, 1P, HPTA), −12.70 (s, 1P, HPTA).

$[Ru^{II}Cl_2(HL3)(HPTA)_2]Cl_2{\cdot}H_2O{\cdot}C_2H_5OH$. Yield 78 mg, 44 %. Found C, 29.9; H, 4.9; N, 16.1; S, 3.7; H_2O + C_2H_5OH 7.8 %. Calc. for $C_{22}H_{44}N_{10}O_5SP_2Cl_4Ru$ C, 30.5; H, 5.1; N, 16.2; S, 3.7; H_2O + C_2H_5OH 7.4 %. $^{31}P\{^1H\}$ NMR (121.4 MHz, D_2O) δ = −11.27 (s, 1P, HPTA), −12.34 (s, 1P, HPTA).

$[Ru^{II}Cl_2(HL4)(HPTA)_2]Cl_2{\cdot}H_2O{\cdot}C_2H_5OH$. Yield 73 mg, 41 %. Found C, 34.5; H, 4.7; N, 15.0; S, 3.5: H_2O + C_2H_5OH 6.6 %. Calc. for $C_{26}H_{44}N_{10}O_5SP_2Cl_4Ru$ C, 34.2; H, 4.8; N, 15.3; S, 3.5; H_2O + C_2H_5OH 7.0 %. $^{31}P\{^1H\}$ NMR (121.4 MHz, D_2O) δ = −11.46 (s, 1P, HPTA), −12.63 (s, 1P,HPTA).

Physicochemical Characterization

C, H, N, and S analyses were performed with a Thermo Scientific Flash 2000 elemental analyzer. Thermogravimetric analysis (TGA) measurements were done on a Shimadzu TGA 50 thermobalance with a platinum cell, working under flowing nitrogen (50 mL min^{-1}) and a heating rate of 0.5 °C min^{-1} (RT −80 °C range) and 1.0 °C min^{-1} (80–350 °C range). Conductometric measurements were performed at 25 °C in 1 mM water solutions using a conductivity meter 4310 Jenway. Fourier transform infrared spectroscopy (FTIR) spectra (4,000–400 cm^{-1}) of the complexes and the free ligands were measured as KBr pellets with a Bomen FTIR model M102 instrument. Electronic spectra were recorded on a Spectronic 3000 spectrophotometer. ^{1}H-NMR and 31P-NMR spectra of the complexes were recorded at 300.13 and 121.4 MHz, respectively, with a Bruker Avance DRX-300 instrument. Experiments were performed at 30 °C in D_2O. Electrochemical behavior was studied by cyclic voltammetry. Cyclic voltammograms were obtained with a Epsilon electrochemical analyzer. A standard electrochemical three-electrode cell of 10-mL volume completed the system. Hanging drop mercury electrode (HDME) was employed as the working electrode. A platinum wire was used as the counter electrode, while a Ag/Ag^+ electrode was used as a reference electrode. Measurements were performed at room temperature in 1 mM DMSO solutions of the complexes using tetrabutylammonium hexafluorophosphate (ca. 0.1 M) as supporting electrolyte. Solutions were deoxygenated via purging with nitrogen for 15 min prior to the measurements. A continuous gas stream was passed over the solution during the measurements.

Lipophilicity Studies

Lipophilicity tests were performed by the "shake flask" methodology determining the partition coefficient (P_{OW}) of the complexes in n-octanol/physiological solution (phosphate buffer pH 7.4, 0.15 M NaCl) [38]. Concentration of Ru complexes in both phases was determined spectrophotometrically by measuring the absorbance at 436 nm. Additionally, lipophilicity was determined by reversed-phase TLC

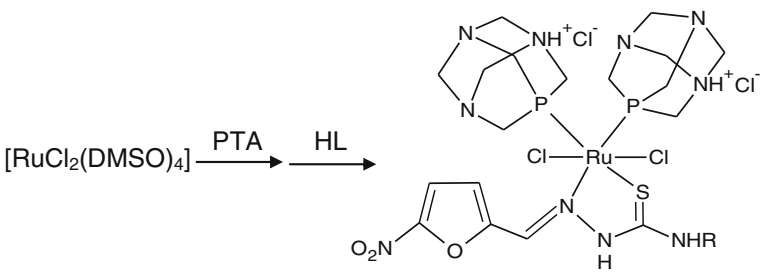

Scheme 1 Synthesis of $[Ru^{II}Cl_2(HL)(HPTA)_2]Cl_2$ complexes

experiments performed on precoated TLC plates SIL RP-18 W/UV254 and eluted with DMSO/physiological serum (60:40 *v*/*v*). Stock solutions were prepared in pure acetone prior to use. The plates were developed in a closed chromatographic tank and dried, and the spots were located under UV light. The R_f values were averaged from three determinations and converted into R_M values via the relationship: $R_M = \log[(1/R_f)-1]$ [27].

Biological Studies

Activity on Dm28c Strain T. cruzi Epimastigotes *T. cruzi* epimastigotes Dm28c strain, from our own collection (Programa de Farmacología Molecular y Clínica, Facultad de Medicina, Universidad de Chile), were grown at 28 °C in Diamond's monophasic medium, as reported earlier, but replacing blood by 4 μM hemin [39]. Heat-inactivated newborn calf serum was added to a final concentration of 4 %. Compounds dissolved in DMSO (1 % final concentration) were added to a suspension of 3×10^6 epimastigotes/mL. Parasite growth was followed by nephelometry. No toxic effect of DMSO alone was observed. From the epimastigote exponential growth curve, the culture growth constant (k) for each compound concentration and for controls was calculated (regression coefficient >0.9, $p<0.05$). This constant corresponds to the slope resulting from plotting the natural logarithm (Ln) of nephelometry lecture versus time [40]. Half maximal inhibitory concentration (IC50) is the drug concentration needed to reduce k in 50 %, and it was calculated by linear regression analysis from the k values and the concentrations used for the experiments. Reported values are the mean of at least three independent experiments.

Viability on T. cruzi (Dm28c Clone) Trypomastigotes Vero cells were infected with *T. cruzi* metacyclic trypomastigotes from 15-day-old Dm28c clone epimastigote cultures. Subsequently, the trypomastigotes harvested from this culture were used to infect further Vero cell cultures at a density of 1×10^6 parasites/25 cm^3. These trypomastigote-infected Vero cell cultures were incubated at 37 °C in humidified air and 5 % CO_2 for 5 to 7 days. After this time, culture media were collected and centrifuged at $3{,}000\times g$ for 5 min. The trypomastigote-containing pellets were resuspended in Roswell Park Memorial Institute Media (RPMI) supplemented with 5 % fetal bovine serum and penicillin-streptomycin at a final density of 1×10^7 parasites/mL. Trypomastigotes of 210×10^6 are equivalent to 1 mg of protein or 12 mg of wet weight. Viability assays were performed by using the 3-(4,5-dimethylthiazol-2-yl)-2,5-diphenyl tetrazolium bromide (MTT) reduction method as previously described [41, 42]. Briefly, 1×10^7 trypomastigotes were incubated in fetal bovine serum-RPMI culture medium at 37 °C for 24 h with and without the Ru complexes under study at 5 to 100 μM final concentrations. An aliquot of the parasite suspension was extracted, and it was incubated in a flat-bottom 96-well plate, and MTT was added at a final concentration of 0.5 mg/mL, incubated at 28 °C for 4 h, and then solubilized with 10 % sodium dodecyl sulfate 0.1 mM HCl and incubated overnight. Formazan formation was measured at 570 nm with the reference wavelength at 690 nm in a multiwell reader (Labsystems Multiskan MS). Untreated parasites were used as negative controls (100 % of viability). Finally, a nonlinear regression analysis, using Log concentration versus normalized response fit, by Graph Pad prism software was performed. Results are reported as IC_{50} values.

In Vitro Amebicide Activity

Parasite Culture E. histolytica HM1-IMSS trophozoites were axenically grown in TYI-S33 medium [43]. Amebas (1×10^5 of live trophozoites) were placed in vials with 3 mL of the TYI-S33 culture media; each coordination compound previously dissolved in DMSO was added to get final concentrations of 100, 50, 10, and 1 μM. Positive controls with metronidazole and negative controls with phosphate buffer solution (PBS) were used.

Viability Amebic trophozoite viability was assessed employing two different methods, (1) vital marker trypan blue and (2) carboxyfluorescein diacetate succinimidyl ester (CFDA-SE) and propidium iodide fluorescent markers. In both methods, the viability counts were done at 24, 48, and 72 h. A hematocytometer was used to realize the parasite counts with trypan blue; meanwhile, counting with fluorescent dyes was done in a fluorescent microscope Olympus BX51 following the instructions provided by the supplier.

Cytotoxicity Assay Against Murine Macrophage RAW 264.7

Macrophage Proliferation Assay The macrophage proliferation index was investigated using the MTT assay. RAW 264.7 cells were seeded in a 96-well plate at a concentration of 3×10^4 cells/well and incubated for 24 h with different concentrations of the compounds, at 37 °C in serum-free medium. Then, the cells were submitted to the MTT assay. The absorbance was measured at 570 nm in a multiwell reader (Asys Expert Plus©, Austria). The relative cell viability was determined by the amount of MTT converted to the insoluble formazan salt. Data are expressed as the mean percentage of viable cells as compared to the respective control cultures treated with solvent.

Mechanism of Action

Free Radical Production in T. cruzi Epimastigotes (Dm28c Strain) The free radical production capacity of the new

complexes was assessed in the parasite by electron paramagnetic resonance (ESR) using 5,5-dimethyl-1-pyrroline-*N*-oxide (DMPO) for spin trapping. Each tested compound was dissolved in DMF (spectroscopy grade) (ca. 1 mM), and the solution was added to a mixture containing the homogenized epimastigote form of *T. cruzi* (Dm28c strain, final protein concentration 4–8 mg/mL) and DMPO (final concentration 250 mM). The mixture was transferred to a 50-μL capillary. ESR spectra were recorded in the X band (9.85 GHz) using a Bruker ECS 106 spectrometer with a rectangular cavity and 50-KHz field modulation. All the spectra were registered in the same scale, after 15 scans [32].

DNA Interaction Studies

Calf Thymus DNA Interaction Studies The complexes were tested for their DNA interaction ability using native calf thymus DNA, (CT DNA) (type I), from Sigma Chemical Co. by a modification of a previously reported procedure [32]. CT DNA was dissolved in water (overnight, ca. 1×10^{-4} mol/mL). Solutions of the complexes in DMSO (1 mL, 10^{-3} M) were incubated at 37 °C with 1 mL of CT DNA solution during 96 h (complex/base pair molar ratio=1). In order to eliminate the unbound complex, DNA/complex mixture was exhaustively washed (treated with ethanol to precipitate DNA and with water to redissolve it). Quantification of bound ruthenium was done by atomic absorption spectroscopy on a Perkin Elmer 380 spectrometer. DNA concentration per nucleotide was determined by UV absorption spectroscopy using the molar absorption coefficient of 6,000 mol^{-1} dm^3 cm^{-1} at 260 nm. Interaction levels were determined as nanomole of Ru bound per milligram of DNA base or as mole of Ru bound per mole of DNA base.

Atomic Force Microscopy (AFM) Studies To optimize the observation of the conformational changes in the tertiary structure of pBR322 plasmid DNA, the plasmid was heated at 60 °C for 30 min to obtain a majority of open circular form. Fifteen nanograms of pBR322 DNA was incubated in an appropriate volume with the required compound concentration corresponding to the molar ratio base pairs (bp)/compound 5:1. Each ruthenium complex was dissolved in a minimal amount of DMSO, and (4-(2-hydroxyethyl)-1-piperazineethanesulfonic acid buffer (HEPES) pH 7.4 was then added up to the required concentration. The different solutions as well as Milli-Q® water were filtered with 0.2-μm FP030/3 filters (Schleicher & Schuell GmbH, Germany). Incubations were carried out at 37 °C for 5 h. Samples were prepared by placing a drop of DNA solution or DNA-compound solution onto mica (TED PELLA, Inc., California, USA). After adsorption for 5 min at room temperature, the samples were rinsed for 10 s in a jet of deionized water (18 $M\Omega cm^{-1}$ from a Milli-Q® water purification system) directed onto the surface. The samples were blow-dried with compressed argon and then imaged by AFM. The samples were imaged by a Nanoscope III Multimode AFM (Digital Instrumentals Inc., Santa Barbara, CA) operating in tapping mode in air at a scan rate of 1–3 Hz. The AFM probe was a 125-mm-long monocrystalline silicon cantilever with integrated conical-shaped Si tips (Nanosensors, GmbH, Germany) with an average resonance frequency f_o=330 KHz and spring constant K=50 N/m. The cantilever was rectangular, and the tip radius given by the supplier was 10 nm, a cone angle of 35°, and with a high aspect ratio. The images were obtained at room temperature (T=23±2 °C), and the relative humidity was usually lower than 40 % [44].

Viscosity Measurements Viscosity experiments were conducted at 25 °C on an automated and viscometer model SV-10. Stock solutions of each complex were prepared in DMSO/water (4:1) and used immediately after preparation. A 1 mM CT DNA solution was diluted 1:4 with TE buffer. For each complex, increasing amounts of complex stock solution were added to this DNA solution to reach complex/DNA molar ratios in the range 0–2.0. The DMSO amount in the samples never exceeded 2 %. After thermal equilibrium was achieved (15 min), the viscosity of each sample was repeatedly measured. Mean values of five measurements performed at intervals of 1 min were used to evaluate the viscosity of each sample.

Fluorescence Studies To a 50-μg/mL CT DNA solution in Milli-Q® water, 30 μL of a 5 mM ethidium bromide solution was added to get a 1:1 molar ratio. The mixture was incubated for 30 min at 37 °C. Increasing amounts of a 1.5 mM DMSO/Milli-Q® water stock solution of the complex under study were added to reach the following final concentrations of the complex: 0, 10, 20, 30, 40, and 50 μM. Fluorescence spectra (λ_{ex}=514 nm) were recorded at room temperature with a HORIBA NanoLog iHR 320 spectrophotometer in the wavelength range 530–670 nm after a short incubation time [45].

Results and Discussion

Characterization

Four new ruthenium complexes with 5-nitrofuryl containing thiosemicarbazones and PTA as ligands have been synthesized and fully characterized. All obtained complexes were very soluble in water (S>10 mM). Complexes of the formula $[Ru^{II}Cl_2(HL)(HPTA)_2]Cl_2{\cdot}H_2O{\cdot}C_2H_5OH$ (Scheme 1) were obtained. Analytical data, including thermogravimetric analysis results, confirmed the proposed formula and the presence of water and ethanol as crystallization solvents. The presence of crystallization ethanol was also confirmed by the presence

of the typical signals at ca. 1.1 ppm (triplet) and 3.6 ppm (quatriplet) in the ^{1}H-NMR spectra of all the complexes (Fig. S1, Supplementary Material).

In the ^{1}H-NMR spectra of all the obtained compounds in D_2O, a complicated pattern of wide signals that would correspond to protons of the thiosemicarbazone ligands was observed between 7.2 and 8.5 ppm. For the PTA ligand, the signals at 3.9 and 4.4 ppm that are observed as a doublet (PC*H*$_2$N) and multiplet (NC*H*$_2$N), respectively, in the free PTA changed to complex broad multiplets at 3.2–3.4 and 4.1–4.6 ppm as a consequence of the formation of the complexes.

One unique feature of PTA ligand is its ability to be regioselectively protonated at nitrogen center forming the ammonium-phosphine $[(H)PTA]^{+}$. Some HPTA complexes of various transition metals have been characterized [33, 34]. The presence of protonated PTA ligands in the obtained complexes was confirmed by different characterization techniques. On one hand, conductivity measurements in 1 mM water solutions showed molar conductivity values in the range of 245–259 Scm^2 mol^{-1}. These values are in accordance with a 1:2 electrolyte [46]. On the other, the *N*-protonation of PTA decreases molecular symmetry of the ligand resulting in a highly complex ^{1}H-NMR spectra with multiple spin systems [33]. This fact was observed in the ^{1}H-NMR spectra in D_2O of all the obtained complexes. In addition, it has been proposed that the presence of crystallization water molecules would favor the stabilization of the protonated ligand by hydrogen bonding formation [33, 34].

^{31}P-NMR spectra of free PTA in D_2O showed a singlet at −95.9 ppm. For the obtained complexes, two signals at around −11.3 and −12.9 ppm were observed (Fig. S2, Supplementary Material). These signals would be in agreement with a *cis* geometry of the HPTA ligands in the complexes [47, 48]. Previously reported *trans* PTARuPTA moiety showed a singlet at around −50 ppm in D_2O or a less negative one, −40 ppm, if HPTA is present [48]. No signals in this spectral zone were observed for the obtained complexes.

The infrared vibrational spectroscopic behavior of all ruthenium complexes was studied in the solid state and compared with that previously reported for the free thiosemicarbazone ligands and their metal complexes [27, 32, 49]. Bands corresponding to both PTA and the thiosemicarbazone ligands confirm their presence in the obtained complexes (Fig. S3, Supplementary Material). Significant infrared vibration bands, useful for determining the ligand mode of coordination, were tentatively assigned for the complexes and are shown in Table 1. After coordination, clear changes in the wavenumber of the υ(C=N) bands of the free thiosemicarbazone ligands, at approximately 1,500–1,600 cm^{-1}, are observed. This modification is consistent with coordination of the thiosemicarbazone ligands through the iminic nitrogen. On the other hand, the shift to higher wave numbers of the υ(N–N) band, has also been related to the electronic delocalization produced as a consequence of coordination through the iminic nitrogen atom [27, 29, 49]. In addition, υ(C=S) bands, at around 820–850 cm^{-1}, should shift to lower wave numbers when thiosemicarbazones act as N,S bidentate ligands, but as it had been previously stated, they could not be unambiguously assigned for the complexes [49]. In agreement with the reported formulae of the complexes, the υ(NH) band, at approximately 3,120–3,150 cm^{-1}, is present in all complexes, indicating that the thiosemicarbazone ligand is nondeprotonated. In addition, an almost identical band shift pattern of the thiosemicarbazone ligands was observed for the obtained complexes in comparison to all previously reported ones that show the ligand in the neutral form [27, 29, 49]. As shown in Table 1, some bands of the PTA ligand were tentatively assigned. As expected, some of them were shifted in the complexes as a consequence of coordination [33, 34, 50].

To our knowledge, only one Ru-thiosemicarbazone-PTA complex $[RuLCl(HPTA)_2]Cl_2{\cdot}C_2H_5OH{\cdot}H_2O$, very similar to that reported here, had been previously obtained with the tridentate 2-acetylpyridine N^4,N^4-dimethylthiosemicarbazone (L) [47].

Cyclic Voltammetry

All ruthenium compounds displayed comparable voltammetric behavior in DMSO solution. Electrochemical processes for both free PTA and thiosemicarbazone ligands could be observed in the complexes (Fig. S4, Supplementary Material). The metal complexes showed two well-defined quasi-reversible waves at around −0.4 and −1.1 V versus Ag/Ag^{+}. The first one corresponds to a PTA-centered reduction process that appears at lower potentials because of ruthenium complexation. The second one, related to the thiosemicarbazone ligand, could be assigned to a process involving a one electron transfer leading to the generation of the anion radical $RNO_2{\cdot}^{-}$ by reduction of the nitro moiety [27, 29, 32].

It had been previously demonstrated that the mechanism of antitrypanosomal action of these nitrofuryl containing thiosemicarbazone ligands is the same as that reported for the reference drug nifurtimox [36]. The first step of this mechanism involves the reduction of the nitro moiety leading to a nitro anion radical that through redox cycling could generate other toxic radical species [31, 36]. In this sense, the redox potential of the nitro group could be a way of predicting how easy this reduction process in vivo could be. Therefore, the effect of ruthenium complexation and the presence of PTA co-ligand on this potential were studied. Results are shown in Table 2. The reduction potentials of the nitro moiety slightly changed as a consequence of the formation of the complexes being the obtained compounds more difficult to reduce than the corresponding ligands.

Table 1 Tentative assignment of the main characteristic IR bands of the ligands and their ruthenium complexes (cm^{-1})

Compound	ν(C=N)	$\nu_s(NO_2)$	ν(N–N)	$\delta(NO_2)$ + furan[a]	PTA
HL1	1,602	1,356	1,108	811	–
$[RuCl_2(HL1)(HPTA)_2]Cl_2$	1,618	1,353	1,160	811	1,311, 1,244, 1,114–1,097, 975, 950, 573
HL2	1,599	1,360	1,120	810	–
$[RuCl_2(HL2)(HPTA)_2]Cl_2$	1,564	1,352	1,163	811	1,308, 1,244, 1,113–1,098, 975, 951, 573
HL3	1,602	1,352	1,104	805	–
$[RuCl_2(HL3)(HPTA)_2]Cl_2$	1,560	1,351	1,152	811	1,313, 1,243, 1,114–1,097, 975, 951, 572
HL4	1,595	1,344	1,104	811	–
$[RuCl_2(HL4)(HPTA)_2]Cl_2$	1,598	1,352	1,209	812	1,311, 1,244, 1,114–1,096, 975, 951, 573

Free PTA ligand bands: ν(CNC) + $\delta(CH_2)$ 1,297 and 1,242 cm^{-1}; δ(CNC) + δ(PCN) 1,105; δ(CNC) + $\rho(PH_2)$ 971 and 952 cm^{-1}; δ(PCN) 582 cm^{-1}

ν stretching, *δ* bending, *ρ* rocking

[a] δ(NO2) + furan modes or furan hydrogen wagging symmetric modes

Although complexation seems to have a negative effect on the nitro moiety potential that could lead to a negative influence on biological activity, the complexes are still more easily bioreducible than the reference drug Nifurtimox.

Lipophilicity Studies

Lipophilicity of the complexes was experimentally determined through the partition coefficient physiological solution/n-octanol, P_{OW}. Due to the very low water solubility of the thiosemicarbazone ligands, P_{OW} could not be determined for these compounds. Therefore, in order to study the effect of the formation of the complex and the presence of the hydrophilic PTA co-ligand on the thiosemicarbazone ligands' physicochemical properties, R_M values were obtained for all the compounds. In such experiments, lipophilicity was experimentally determined using reversed-phase TLC where the stationary phase (precoated TLC-C18) may be considered to simulate lipids of biological membranes or receptors, and the mobile phase (DMSO/physiological serum 60:40 *v*/*v*) resembles the aqueous biological milieu. The composition of the mobile phase was adjusted in order to allow differentiating complexes according to their lipophilicity [27]. Results are shown in Table 2.

Table 2 Reduction potentials of the nitro moiety and lipophilicity values of the obtained ruthenium complexes and the corresponding ligands

Compound	Couple $NO_2/NO_2^{\cdot -}$		P_{ow}[d]	R_M[e]
	Ep_c [a,c] (V)	Ep_a [b,c] (V)		
HL1	−1.10	−1.00	–	−1.2
$[RuCl_2(HL1)(HPTA)_2]Cl_2$	−1.14	−1.10	1.0	−0.5
HL2	−1.09	−1.00	–	−0.6
$[RuCl_2(HL2)(HPTA)_2]Cl_2$	−1.11	−1.00	1.4	0.7
HL3	−1.11	−1.02	–	−0.5
$[RuCl_2(HL3)(HPTA)_2]Cl_2$	−1.11	−1.01	2.3	0.8
HL4	−1.07	−0.99	–	−0.1
$[RuCl_2(HL4)(HPTA)_2]Cl_2$	−1.11	−1.00	4.8	1.1
Nifurtimox	−1.17	−1.11	–	–

[a] Cathodic peak potential

[b] Anodic peak potential

[c] Redox potentials measured in DMSO at 100 mV/s versus Ag/Ag+ electrode

[d] Partition coefficient n-octanol/physiological solution

[e] $R_M = \log [(1/R_f) - 1]$, elution mixture DMSO/physiological serum 60:40 *v*/*v*

All obtained complexes were more lipophilic than the corresponding thiosemicarbazone ligands in spite of the presence of the hydrophilic PTA ligand in the complexes. Obtained R_M values were similar to those previously reported for $[RuCl_2(HL)_2]$ complexes [27]. As expected, the lipophilicity of the obtained complexes increases as the *N*-substituent in the thiosemicarbazone ligand changes from H to phenyl. $[RuCl_2(HL4)(HPTA)_2]Cl_2$ complex, having the most lipophilic ligand, was also the most lipophilic complex.

Biological Results

The stability of solutions of the complexes in DMSO and in water was determined by UV-visible spectrophotometry and conductivity measurements for 10 days. Complexes were stable during the studied period; no changes in the visible spectra or in the molar conductivity values were detected.

In Vitro anti-T. cruzi Activity

The complexes in vitro activities against epimastigotes of *T. cruzi* (Dm28 c strain) were evaluated as a preliminary screening assay (Table 3). Obtained complexes resulted less toxic to the epimastigote form of the parasite than Nifurtimox, being all of them less active than the corresponding free

Table 3 In vitro activity against *T. cruzi* epimastigotes and trypomastigotes (Dm28c clone), *E. histolytica* HM1:IMSS trophozoites and cytotoxicity on RAW 264.7 murine macrophages of the ligands and the obtained ruthenium complexes

Compound	IC_{50}/μM macrophages	*T. cruzi*		IC_{50}/μM *E.histolytica*
		IC_{50}/μM epimastigotes	IC_{50}/μM trypomastigotes	
HL1	10.2±0.7	11.8±2.9[a]	9.8±1.5[a]	>100
$[RuCl_2(HL1)(HPTA)_2]Cl_2$	>200	>100	>100	>100
HL2	20.5±0.2	11.9±1.7[a]	17.4±1.9[a]	>100
$[RuCl_2(HL2)(HPTA)_2]Cl_2$	>200	>100	>100	>100
HL3	22.8±0.8	15.9±2.8[a]	18.5±1.7[a]	>100
$[RuCl_2(HL3)(HPTA)_2]Cl_2$	>200	>100	>100	> 100
HL4	57.8±1.2	9.5±1.6[a]	22.7±1.6[a]	>100
$[RuCl_2(HL4)(HPTA)_2]Cl_2$	>200	84.2±1.3	85.2±1.9	5.2±0.4
Nifurtimox	266.0±1.1	22.8±0.7	20.1±0.8	–
Metronidazole	–	–	–	6.8±0.2

Results are the means of three different experiments

[a] Data from reference [23]

thiosemicarbazone ligands. $[RuCl_2(HL4)(HPTA)_2]Cl_2$ complex was the most active one (IC_{50}=84.21 μM). It is known that the activity against one form of the parasite life cycle does not mean a similar activity against the other forms due to the metabolic changes that occur during transformation between forms along the biological cycle. Therefore, all complexes were tested for their activity against the infective trypomastigote form of the parasite. Results are depicted in Table 3. In this case, similar results were obtained for both parasite forms, the complex $[RuCl_2(HL4)(HPTA)_2]Cl_2$ being the most active compound with similar IC_{50} values (84.21 μM for epimastigotes and 85.23 μM for the trypomastigote form).

A decrease in the anti-*T. cruzi* activity as a consequence of ruthenium complexation had just been observed for other ruthenium 5-nitrofuryl thiosemicarbazone complexes [23, 27]. For some of them, the poor activity had been correlated with solubility and/or lipophilicity problems [27]. This correlation was not observed for $[RuCl_2(HL)(HPTA)_2]Cl_2$ complexes that are water soluble and present similar lipophilicity to that of other more active ruthenium compounds. However, as previously observed, the most lipophilic complex $[RuCl_2(HL4)(HPTA)_2]Cl_2$ turned out to be the most active one.

In Vitro Amebicide Activity

In vitro amebicide activity of ruthenium compounds was studied in a cell culture of trophozoites HM1:IMSS. Positive controls with metronidazole and negative controls with PBS were used. Results are depicted in Table 3.

Results clearly showed the inefficacy of free thiosemicarbazone ligands to inhibit the proliferation of *E. histolytica* trophozoites in vitro. The same behavior was observed for $[RuCl_2(HL1)(HPTA)_2]Cl_2$ and $[RuCl_2(HL2)(HPTA)_2]Cl_2$ coordination compounds with maximum growth inhibition of 10 % at final concentration of 100 μM. $[RuCl_2(HL3)(HPTA)_2]Cl_2$ presented an increase in antiproliferative activity reaching 25 % of culture inhibition after 24-h incubation. The effect is conserved at 48 and 72 h with no evidence of culture recovery. The antiproliferative activity exhibited by the compound $[RuCl_2(HL4)(HPTA)_2]Cl_2$ is really important since 24 h of incubation and even the lower doses (1 μM) produced 30 % of culture inhibition. The graph shown in Fig. S5, Supplementary Material, suggests a dose-dependent behavior, with the maximum effect reached after 24 h of incubation and conserved till the end of the experiment. The IC_{50} calculated for this compound is 5.2±0.4 μM, value slightly lower than the observed for the first choice drug metronidazole (6.8±0.2 μM).

Cytotoxicity on RAW 264.7 Murine Macrophages

The specificity of the antiparasitic activity of the obtained ruthenium compounds and the thiosemicarbazone ligands was evaluated by analyzing their cytotoxicity against a murine macrophage-like cell line (RAW 264.7). Results are shown in Table 3. The 5-nitrofuryl containing thiosemicarbazones were very toxic against these mammalian cells. On the other hand, obtained ruthenium complexes were not cytotoxic. These results account for the fact that $[RuCl_2(HL4)(HPTA)_2]Cl_2$ turned out to be selective for both *T. cruzi* and *E. histolytica* parasites with an excellent selectivity index ($SI = IC_{50\ macrophages}/IC_{50\ parasite}$) for *E. histolytica* (SI>38).

Mechanism of Action

Free Radical Production in T. cruzi

The mechanism of anti-*T. cruzi* action of the 5-nitrofuryl containing thiosemicarbazones involves bioreduction and the

production of toxic free radical species. This mechanism of action seems to remain for other previously reported metal complexes of these bioactive ligands [23, 25, 28–32]. Therefore, the free radical production capacity of the obtained ruthenium compounds was assessed by EPR incubating the compounds with *T. cruzi* (Dm28c strain) epimastigotes. In order to detect possible intracelullar free radical species having short half-lives, DMPO was added as spin trapping agent. All complexes showed a similar line pattern on the EPR spectra. As an example, the EPR spectrum for $[RuCl_2(HL4)(HPTA)_2]Cl_2$ complex is shown in Fig. 2.

A thirteen-line spectral pattern was observed for all ruthenium complexes corresponding to three different DMPO spin adducts. One of the detected spin adducts (“) corresponds to the trapping of a carbon-centered radical by DMPO (a_N=15.0 G, a_H=22.5 G) [51]. This spin adduct could be related to the bioreduction of the complexes and the formation of a DMPO-nitroheterocyclic radical species. In addition, intracellular hydroxyl radical species that could arise due to redox cycling processes was also observed in low concentration. The corresponding DMPO-OH spin adduct (*) consists of four lines of 1:2:2:1 intensities (a_N = a_H = 15 G) [51]. The third line pattern (#) could be related to the oxidation of the spin trap and/or the rapid decomposition of DMPO-OH adduct [51, 52].

These results confirm that all compounds were capable of producing free radicals and oxidative stress in the parasite even though the redox potential of the nitro moiety was less favorable than for the free ligands. Difficulties of the complexes in trespassing the parasitic membrane by irreversible interaction of the compounds with the proteins in the culture media could explain their poor observed anti-*T. cruzi* activity. A similar behavior had been previously observed for other ruthenium complexes [18].

Morphological Changes in E. histolytica Trophozoites

Once the cells were exposed to $[RuCl_2(HL4)(HPTA)_2]Cl_2$ for 24 h, morphological changes in trophozoites like adoption of cellular rounding and shrinkage could be observed. These morphological changes were also observed in *E. histolytica* cultures exposed to oxidative stress inductors like aminoglycoside G418 [53], hydrogen peroxide [54, 55], other nitric oxide species [56] and first row transition metals coordination compounds [57]. None of these changes was observed when the parasites were exposed to commonly used antiparasitic compounds such as metronidazole, benzimidazole, mebendazole, albendazole, niclosamide [58, 59], and nonredox active Zn coordination compounds [57, 60]. Authors of the mentioned studies corroborate the apoptosis-like processes and agree with Huppertz in that reduction in cell size and shrinkage of the cytoplasm are two of the most reliable morphological criteria for defining programmed cell death (PCD) processes [61]. In addition, cell volume decreases and DNA damage can be observed in trophozoites cultures stained with the fluorescent markers CFDA-SE and propidium iodide (PI) (Fig. 3). CFDA-SE is colorless and nonfluorescent until its acetate groups are cleaved by intracellular esterases to yield highly green fluorescence. On the other hand, PI has a very intense red fluorescence when it interacts with DNA, which only happens when nuclear membrane is significantly damaged and the genetic material is exposed. For control culture, trophozoites have an intense green

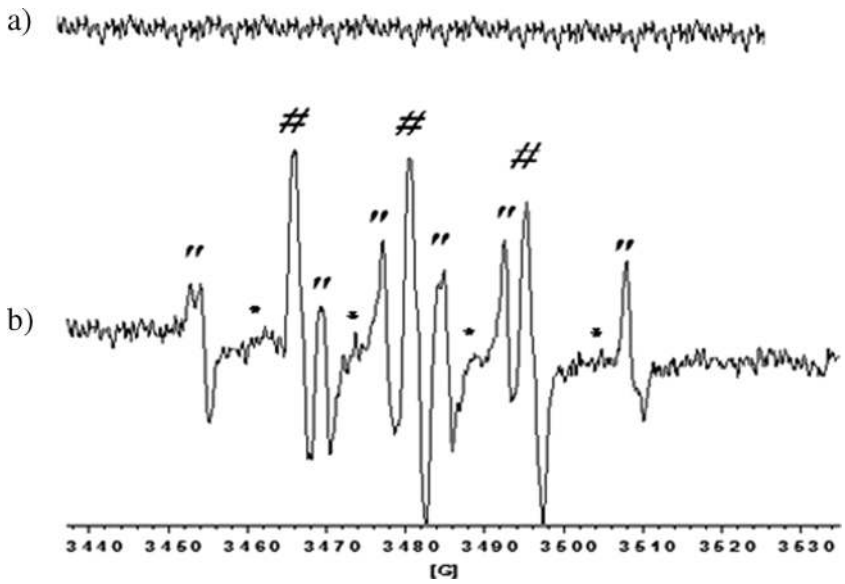

Fig. 2 **a** Control EPR spectrum (without metal complex). **b** EPR spectrum obtained after 5-min incubation of $[RuCl_2(HL4)(HPTA)_2]Cl_2$ (1 mM) with *T. cruzi* epimastigotes (Dm28c strain, final protein concentration of 4–8 mg/mL), NADPH (1 mM), and DMPO (100 mM). “ characteristic signals of DMPO-nitrocompound spin adduct, * characteristic signals of DMPO-OH spin adduct, # DMPO or DMPO-OH oxidation signals

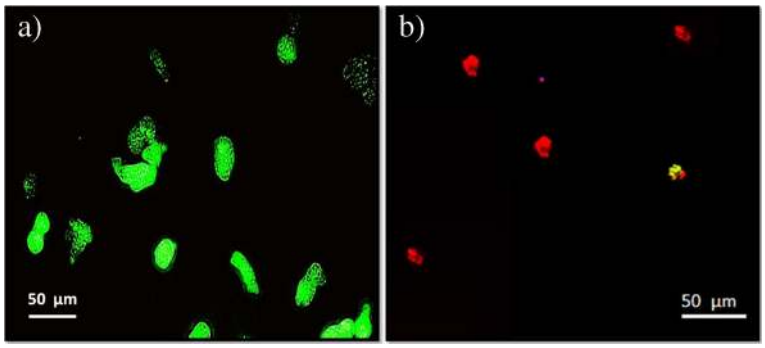

Fig. 3 Fluorescence image of *E. histolytica* trophozoites: **a** control culture and **b** culture incubated 24 h with 10 µM of $[RuCl_2(HL4)(HPTA)_2]Cl_2$

fluorescence with cellular size between 25 and 40 µm (Fig. 3a). Meanwhile, trophozoites exposed to 10 µM of $[RuCl_2(HL4)(HPTA)_2]Cl_2$ for 48 h show only red color, indicating interaction of the fluorescent marker with the DNA due to severe cell damage (Fig. 3b).

Cellular size is also confirmed with the data obtained from TC10 automated cell counter of Bio-Rad (Fig. S6, Supplementary Material). Trophozoite size range without treatment is 22 to 40 µm. Once the culture is incubated for 24 h with 10 µM of $[RuCl_2(HL4)(HPTA)_2]Cl_2$, an important size decrease is observed, reaching only 5 µm. This size is not only observed in dead trophozoites but also in alive ones, suggesting an irreparable damage in cells that are still alive.

All these results suggest that $[RuCl_2(HL4)(HPTA)_2]Cl_2$ exert an important cellular damage, probably due to the production of ROS. ROS production could explain the morphological changes in trophozoite cultures and could be the trigger of apoptosis-like processes.

DNA Interaction Studies

Quantification of Calf Thymus DNA Binding

In order to preliminary address if the interaction with DNA could be part of the mode of action of the obtained ruthenium complexes, experiments with calf thymus DNA (CT DNA) were carried out. Binding of all ruthenium complexes to DNA was studied by combining atomic absorption determinations (for the metal) and electronic absorption measurements for DNA quantification. All complexes are very good binding agents for CT DNA (Table 4). The observed ruthenium to DNA binding levels is similar or higher than that reported for antitumor metal complexes having DNA as molecular target and than other previously reported anti-*T. cruzi* agents [23–25, 28, 29, 32, 62].

Fluorescence, Viscosity, and AFM Results

In order to get insight into the mode of interaction between ruthenium complex and DNA, ethidium bromide (EtBr) competitive binding fluorescence experiments were carried out. This experiment is based on the fluorescence generated when EtBr intercalates between the DNA base pairs. If the assayed compound is able to modify EtBr binding, increasing concentrations of it would result in a reduction of fluorescence intensity. This effect was observed for all the obtained ruthenium complexes as it is shown in Fig. 4b for $[RuCl_2(HL4)(HPTA)_2]Cl_2$. The quenching of the emission maximum with increasing concentrations of the ruthenium complex indicates that a deactivation of the adduct's excited state occurs. This deactivation may occur due to a competition between the ruthenium complex and EtBr for the intercalating binding sites in DNA. However, changes in DNA configuration could also alter EtBr binding [63].

The effect of a compound on DNA viscosity is also indicative of its binding mode to DNA in solution.

Table 4 Interaction of ruthenium complexes with calf thymus DNA after 96-h incubation at 37 °C

Compound	Metal/base[a]	Base/metal	nmolRu/mg DNA
$[RuCl_2(HL1)(HPTA)_2]Cl_2$	0.0344±0.0028	29.2±2.4	104.3±8.6
$[RuCl_2(HL2)(HPTA)_2]Cl_2$	0.0385±0.0002	25.3±0.2	119.8±0.7
$[RuCl_2(HL3)(HPTA)_2]Cl_2$	0.0382±0.0008	26.1±0.5	116.0±2.3
$[RuCl_2(HL4)(HPTA)_2]Cl_2$	0.0355±0.0024	29.0±2.0	104.8±3.6

[a] mol ruthenium per mol DNA base

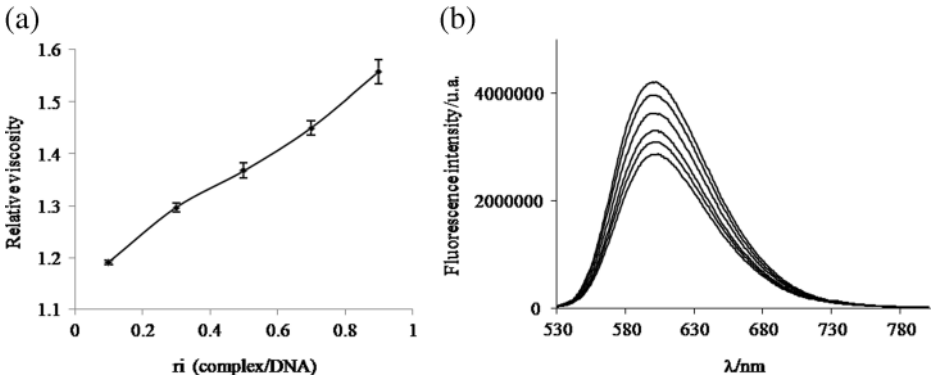

Fig. 4 **a** Relative viscosity versus r_i curve for compound $[RuCl_2(HL3)(HPTA)_2]Cl_2$ (r_i = mol of complex/mol of DNA base pairs). **b** Fluorescence measurements (*a.u.* arbitrary units) for increasing concentrations of $[RuCl_2(HL4)(HPTA)_2]Cl_2$ complex

Viscosity measurements are considered the most important tools when studying the mode of DNA interaction. Viscosity is sensitive to length change of DNA. In this sense, an intercalation mode of interaction lengthens the DNA helix, as base pairs are separated to accommodate the binding ligand, leading to the increase of DNA viscosity. In contrast, other modes of interaction, including covalent binding, could bend (or kink) the DNA helix, reducing its effective length and, hence, its viscosity [64–66]. In order to further elucidate the DNA binding mode of the obtained ruthenium complexes, viscosity measurements were carried out on CT DNA by varying the r_i (r_i = mol of complex/mol of DNA base pairs) values. All the studied complexes increased the viscosity of CT DNA solutions in a concentration-dependent manner. Results for compound $[RuCl_2(HL3)(HPTA)_2]Cl_2$ are shown in Fig. 4a, as an example. These results are in accordance with those obtained in the fluorescence experiments.

AFM has proved to be a useful tool for imaging DNA and also DNA interactions with metal complexes [25, 67]. Ruthenium complexes were incubated with pBR322 plasmid DNA. Obtained AFM images are depicted in Fig. 5. Different extent of changes in the shape of plasmid DNA were observed as a consequence of the supercoiling induced by the ruthenium compounds. The observed effect is clearly more pronounced for $[RuCl_2(HL4)(HPTA)_2]Cl_2$. The very intense modifications of DNA tertiary structure for this complex can be visualized as DNA balls formation (see Fig. 5d).

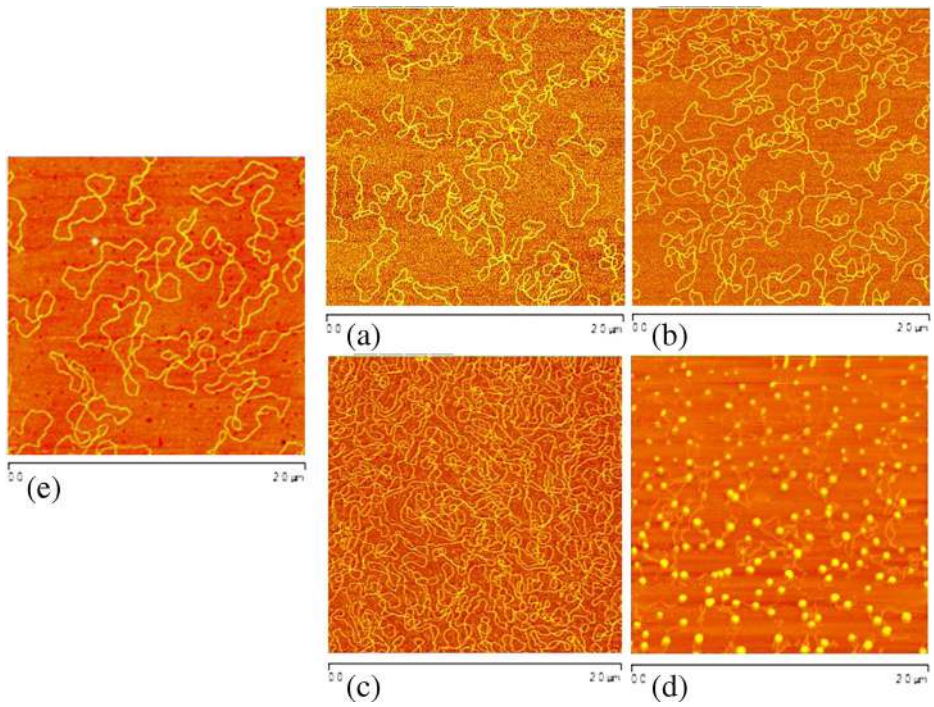

Fig. 5 AFM images showing the modifications suffered by pBR322 DNA due to interaction with the Ru compounds: **a** $[RuCl_2(HL1)(HPTA)_2]Cl_2$, **b** $[RuCl_2(HL2)(HPTA)_2]Cl_2$, **c** $[RuCl_2(HL3)(HPTA)_2]Cl_2$, **d** $[RuCl_2(HL4)(HPTA)_2]Cl_2$ for molar ratio compound: DNA base pairs 1:5 and 5-h incubation at 37 °C, and **e** no metal compound added.

Conclusions

In the search for potential antiparasitic metal complexes, four new ruthenium complexes of the formula $[Ru^{II}Cl_2(HL)(HPTA)_2]Cl_2$ with 5-nitrofuryl containing thiosemicarbazones as bioactive ligand and PTA (1,3,5-triaza-7-phosphaadamantane) as co-ligand were obtained. The effect of the presence of the hydrophilic phosphine PTA resulted evident as obtained compounds were very soluble in water. $[RuCl_2(HL4)(HPTA)_2]Cl_2$ was the most active complex against both *T. cruzi* and *E. histolytica* parasites showing an excellent activity against the last one, even higher than that of the reference drug metronidazole. This complex also turns out to be selective for the parasites, as it was not cytotoxic against murine macrophages (SI>38).

Related to the mechanism of action, obtained compounds were able to produce toxic ROS in both parasites. In addition, complexes were able to interact with DNA in an intercalative-like mode according to the obtained results. This work could be considered a contribution in the search for compounds that could be active against multiple parasites.

Acknowledgments Authors wish to thank CYTED through network 209RT0380, ANII-Uruguay (project FCE_2007_188) and Fondecyt 11080166 and Fondecyt International Cooperation Project 1110029 Chile for the financial support. CS thanks ANII-Uruguay for the research grant Be_INI_2010_1864. Authors also thank Prof. Jorge Castiglioni for the thermal analysis experiments.

References

1. Beaumier CM, Gillespie PM, Hotez PJ, Bottazzi ME (2013) New vaccines for neglected parasitic diseases and dengue. Transl Res 162(3):144–155
2. Liese B, Rosenberg M, Schratz A (2010) Programs, partnerships, and governance for elimination and control of neglected tropical diseases. Lancet 375:67–76
3. Astelbauer F, Walochnik J (2011) Antiprotozoal compounds: state of the art and new developments. Int J Antimicrob Agents 38:118–124
4. Stanley SL Jr (2003) Amoebiasis. Lancet 361:1025–1034
5. Ximénez C, Morán P, Rojas L, Valadez A, Gómez A, Ramiro M, Cerritos R, González E, Hernández E, Oswaldo P (2011) Novelties on amoebiasis: a neglected tropical disease. J Global Infect Dis 3: 166–174
6. Rassi A Jr, Rassi A, Marin-Neto JA (2010) Chagas disease. Lancet 375:1388–1402
7. Rodrigues Coura J, Borges-Pereira J (2010) Chagas disease: 100 years after its discovery. A systemic review. Acta Trop 115:5–13
8. Chaudhary K, Roos DS (2005) Protozoan genomics for drug discovery. Nat Biotechnol 23:1089–1091
9. Urbina JA (2010) Specific chemotherapy of Chagas disease: relevance, current limitations and new approaches. Acta Trop 115:55–68
10. Merlino A, Gonzalez M, Cerecetto H (2010) Targets for anti-T. cruzi drugs in the post-genomic era. Curr Enzym Inhib 6:195–210
11. Le Loup G, Pialoux G, Lescure FX (2011) Update in treatment of Chagas disease. Curr Opin Infect Dis 24:428–434
12. Singh S, Bharti N, Mohapatra PP (2009) Chemistry and biology of synthetic and naturally occurring antiamoebic agents. Chem Rev 109:1900–1947
13. Navarro M, Gabbiani G, Messori L, Gambino D (2010) Metal-based drugs for malaria, trypanosomiasis and leishmaniasis. Recent achievements and perspectives. Drug Discov Today 15:1070–1077
14. Gambino D (2011) Potentiality of vanadium compounds as anti-parasitic agents. Coord Chem Rev 255:2193–2203
15. Sánchez-Delgado RA, Anzellotti A (2004) Metal complexes as chemotherapeutic agents against tropical diseases: trypanosomiasis, malaria and leishmaniasis. Mini-Rev Med Chem 4:22–30
16. Navarro M (2009) Gold complexes as potential anti-parasitic agents. Coord Chem Rev 253:1619–1626
17. Fricker SP, Mosi RM, Cameron BR, Baird I, Zhu Y, Anastassov V, Cox J, Doyle PS, Hansell E, Lau G, Langille J, Olsen M, Qin L, Skerlj R, Wong RSY, Santucci Z, McKerrow JH (2008) Metal compounds for the treatment of parasitic diseases. J Inorg Biochem 102:1839–1845
18. Gambino D, Otero L (2012) Perspectives on what ruthenium-based compounds could offer in the development of potential antiparasitic drugs. Inorg Chim Acta 393:103–114
19. Bahl D, Athar F, Pereira Soares MB, Santos de Sá M, Magalhães Moreira DR, Srivastava RM, Lima Leite AC, Azam A (2010) Structure–activity relationships of mononuclear metal–thiosemicarbazone complexes endowed with potent antiplasmodial and antiamoebic activities. Bioorg Med Chem 18:6857–6864
20. Beraldo H, Gambino D (2004) The wide pharmacological versatility of semicarbazones, thiosemicarba-zones and their metal complexes. Mini Rev Med Chem 4:31–39
21. Lobana TS, Sharma R, Bawa G, Khanna S (2009) Bonding and structure trends of thiosemicarbazone derivatives of metals—an overview. Coord Chem Rev 253:977–1055
22. Greenbaum DC, Mackey Z, Hansell E, Doyle P, Gut J, Caffrey CR, Lehrman J, Rosenthal PJ, McKerrow JH, Chibale K (2004) Synthesis and structure−activity relationships of parasiticidal thiosemicarbazone cysteine protease inhibitors against Plasmodium falciparum, Trypanosoma brucei, and Trypanosoma cruzi. J Med Chem 47:3212–3219
23. Demoro B, Rossi M, Caruso F, Liebowitz D, Olea-Azar C, Kemmerling U, Maya JD, Guiset H, Moreno V, Pizzo C, Mahler G, Otero L, Gambino D (2013) Potential mechanism of the anti-trypanosomal activity of organoruthenium complexes with bioactive thiosemicarbazones. Biol Trace Elem Res 153(1–3):371–381
24. Demoro B, Sarniguet C, Sánchez-Delgado R, Rossi M, Liebowitz D, Caruso F, Olea-Azar C, Moreno V, Medeiros A, Comini MA, Otero L, Gambino D (2012) New organoruthenium complexes with bioactive thiosemicarbazones as co-ligands: potential anti-trypanosomal agents. Dalton Trans 41:1534–1543
25. Vieites M, Smircich P, Pagano M, Otero L, Luane F, Terenzi H, Prieto MJ, Moreno V, Garat B, Gambino D (2011) DNA as molecular target of analogous palladium and platinum anti-Trypanosoma cruzi compounds: a comparative study. J Inorg Biochem 105:1704–1711
26. Merlino A, Otero L, Gambino D, Coitiño EL (2011) In search of patterns over physicochemical properties and pharmacological activities for a set of $[MCl_2(thiosemicarbazone)]$ complexes (M = Pt/Pd): support for multiple mechanisms of antichagasic action excluding DNA-bonding in vivo? Eur J Med Chem 46(7):2639–2651
27. Pagano M, Demoro B, Toloza J, Boiani L, González M, Cerecetto H, Olea-Azar C, Norambuena E, Gambino D, Otero L (2009) Effect of ruthenium complexation on trypanocidal activity of 5-nitrofuryl containing thiosemicarbazones. Eur J Med Chem 44:4937–4943
28. Vieites M, Otero L, Santos D, Olea-Azar C, Norambuena E, Aguirre G, Cerecetto H, González M, Kemmerling U, Morello A, Maya JD, Gambino D (2009) Platinum-based complexes of bioactive 3-(5-nitrofuryl)acroleine thiosemicarbazones showing anti-Trypanosoma cruzi activity. J Inorg Biochem 103(3):411–418

29. Vieites M, Otero L, Santos D, Gajardo D, Toloza J, Figueroa R, Norambuena E, Olea-Azar C, Aguirre G, Cerecetto H, González M, Morello A, Maya JD, Garat B, Gambino D (2008) Platinum(II) metal complexes as potential anti-Trypanosoma cruzi agents. J Inorg Biochem 102:1033–1043
30. Otero L, Maya JD, Morello A, Rigol C, Barriga G, Rodriguez J, Folch C, Norambuena E, Gonzalez M, Olea-Azar C, Cerecetto H, Gambino D (2008) Insight into the bioreductive mode of action of antitrypanosomal 5-nitrofuryl containing thiosemicarbazones. Med Chem 4(1):11–17
31. Otero L, Folch C, Barriga G, Rigol C, Opazo L, Vieites M, Gambino D, Cerecetto H, Norambuena E, Olea-Azar C (2008) ESR, electrochemical and reactivity studies of antitrypanosomal palladium thiosemicarbazone complexes. Spectrochim. Acta Part A 70: 519–523
32. Otero L, Vieites M, Boiani L, Denicola A, Rigol C, Opazo L, Olea-Azar C, Maya JD, Morello A, Krauth-Siegel RL, Piro OE, Castellano E, González M, Gambino D, Cerecetto H (2006) Novel antitrypanosomal agents based on palladium nitrofurylthiosemicarbazone complexes: DNA and redox metabolism as potential therapeutic targets. J Med Chem 49:3322–3331
33. Phillips AD, Gonsalvi L, Romerosa A, Vizza F, Peruzzini M (2004) Coordination chemistry of 1,3,5-triaza-7-phosphaadamantane (PTA): transition metal complexes and related catalytic, medicinal and photoluminescent applications. Coord Chem Rev 248:955–993
34. Bravo J, Bolaño S, Gonsalvi L, Peruzzini M (2010) Coordination chemistry of 1,3,5-triaza-7-phosphaadamantane (PTA) and derivatives. Part II. The quest for tailored ligands, complexes and related applications. Coord Chem Rev 254:555–607
35. Bergamo A, Gaiddon C, Schellens JHM, Beijnen JH, Sava G (2012) Approaching tumour therapy beyond platinum drugs: status of the art and perspectives of ruthenium drug candidates. J Inorg Biochem 106: 90–99
36. Aguirre G, Boiani L, Cerecetto H, González M, Denicola A, Otero L, Gambino D, Rigol C, Olea-Azar C, Faundez M (2004) In vitro activity and mechanism of action against the protozoan parasite Trypanosoma cruzi of 5-nitrofuryl containing thiosemicarbazones. Bioorg Med Chem 12:4885–4893
37. Evans I, Spencer A, Wilkinson GJ (1973) Dichlorotetrakis(dimethyl sulphoxide)ruthenium(II) and its use as a source material for some new ruthenium(II) complexes. Chem Soc Dalton Trans 2:204–209
38. Hansch C, Leo A (1995) The hydrophobic parameter: Measurement and calculation, exploring QSAR. Fundamentals and Applications in Chemistry and Biology. American Chemical Society, Washington, pp 97–124
39. Maya JD, Morello A, Repetto Y, Tellez R, Rodriguez A, Zelada U, Puebla P, Bontá M, Bollo S, San Feliciano A (2000) Effects of 3-chloro-phenyl-1,4-dihydropyridine derivatives on Trypanosome cruzi epimastigotes. Comp Biochem Physiol C 125:103–109
40. Cuellar MA, Salas C, Cortés MJ, Morello A, Maya JD, Preite MD (2003) Synthesis and in vitro trypanocide activity of several polycyclic drimane-quinone derivatives. Bioorg Med Chem 11:2489–2497
41. Muelas-Serrano S, Nogal-Ruiz JJ, Gómez-Barrio A (2000) Setting of a colorimetric method to determine the viability of Trypanosoma cruzi epimastigotes. Parasitol Res 86:999–1002
42. Faundez M, Pino L, Letelier P, Ortiz C, López R, Seguel C, Ferreira J, Pavani M, Morello A, Maya JD (2005) Buthionine sulfoximine increases the toxicity of nifurtimox and benznidazole to Trypanosoma cruzi. Antimicrob Agents Chemother 49:126–130
43. Diamond L (1961) Axenic cultivation of Entamoeba histolytica. Science 134:336–337
44. Benítez J, Guggeri L, Tomaz I, Costa Pessoa J, Moreno V, Lorenzo J, Avilés FX, Garat B, Gambino D (2009) A novel vanadyl complex with a polypyridyl DNA intercalator as ligand: a potential anti-protozoa and anti-tumor agent. J Inorg Biochem 103:1386–1394
45. Zhang G, Guo J, Pan J, Chen X, Wang J (2009) Spectroscopic studies on the interaction of morin–Eu(III) complex with calf thymus DNA. J Mol Struct 923:114–119
46. Geary WJ (1971) The use of conductivity measurements in organic solvents for the characterisation of coordination compounds. Coord Chem Rev 7:81–122
47. Grguric-Sipka S, Kowol CR, Valiahdi S, Eichinger R, Jakupec MA, Roller A, Shova S, Arion VB, Keppler BK (2007) Ruthenium(II) complexes of thiosemicarbazones: the first water-soluble complex with pH-dependent antiproliferative activity. Eur J Inorg Chem 18: 2870–2878
48. Mebi CA, Frost BJ (2007) Isomerization of trans-[Ru(PTA)4Cl2] to cis-[Ru(PTA)4Cl2] in water and organic solvent: revisiting the chemistry of [Ru(PTA)4Cl2]. Inorg Chem 46:7115–7120
49. Gambino D, Otero L, Vieites M, Boiani M, Gonzalez M, Baran EJ, Cerecetto H (2007) Vibrational spectra of palladium 5-nitrofuryl thiosemicarbazone complexes: experimental and theoretical study. Spectrochim Acta Part A 68:341–348
50. Jogun K, Stezowski JJ, Fluck E, Weidlein J (1978) Molecular structure of p-substituted 1,3,5-triaza-7-phosphaadamantanes: vibration spectra and crystal structure analyses. Phosphorous Sulfur 4:99–204
51. Makino K, Hagiwara T, Murakami A (1991) Fundamental-aspects of spin trapping with Dmpo. Radiat Phys Chem 37:657–665
52. Aguilera-Venegas B, Olea-Azar C, Arán V, Maya JD, Kemmerling U, Speisky H, Mendizábal F (2012) Electrochemical, ESR and theoretical insights into the free radical generation by 1,1'-hydrocarbylenebisindazoles and its evaluation as potential bioactive compounds. Int J Electrochem Sci 7:5837–5863
53. Villalba JD, Gómez C, Medel O, Sánchez V, Carrero JC, Shibayama M, Pérez DG, Ishiwara (2007) Programmed cell death in Entamoeba histolytica induced by the aminoglycoside G418. Microbiology 153: 3852–3863
54. Aguilar-Díaz H, Díaz-Gallardo M, Laclette JP, Carrero JC (2010) In vitro induction of Entamoeba histolytica cyst-like structures from trophozoites. PLoS Negl Trop Dis 4:e607
55. Nandi N, Sen A, Banerjee R, Kumar S, Kumar V, Ghosh AN, Das P (2010) Hydrogen peroxide induces apoptosis-like death in Entamoeba histolytic trophozoites. Microbiology 156:1926–1941
56. Ramos E, Olivos-García A, Nequiz M, Saavedra E, Tello E, Saralegui A, Montfort I, Pérez Tamayo R (2007) Entamoeba histolytica: apoptosis induced in vitro by nitric oxide species. Exp Parasitol 116:257–265
57. García-Ramos JC, Toledano-Magaña Y, Talavera-Contreras LG, Flores-Álamo M, Ramírez-Delgado V, Morales-León E, Ortiz-Frade L, Grizett Gutiérrez A, Vázquez-Aguirre A, Mejía C, Carrero JC, Laclette JP, Moreno-Esparza R, Ruiz-Azuara L (2012) Potential cytotoxic and amoebicide activity of first row transition metal compounds with 2,9-bis-(2′,5′-diazahexanyl)-1,1-phenanthroline (L1). Dalton Trans 41:10164–10174
58. Freeman CD, Klutman NE, Lamp KC (1997) Metronidazole. A therapeutic review and update. Drugs 54:679–708
59. Bansal D, Malla N, Mahajan MC (2006) Drug resistance in amoebiasis. Indian J Med Res 123:115–118
60. Zambrano-Villa S, Rosales-Borjas D, Carrero JC, Ortiz-Ortiz L (2002) How protozoan parasites evade the immune response. Trends Parasitol 18:272–278
61. Huppertz B, Frank HG, Kaufmann P (1999) The apoptosis cascade—morphological and immunohistochemical methods for its visualization. Anat Embryol 200:1–18
62. Gómez-Quiroga A, Navarro-Ranninger C (2004) Contribution to the SAR field of metallated and coordination complexes: studies of the palladium and platinum derivatives with selected thiosemicarbazones as antitumoral drugs. Coord Chem Rev 248:119–133
63. Mahadevan S, Palaniandavar M (1998) Spectral and electrochemical behavior of copper(ii)−phenanthrolines bound to calf thymus DNA. $[(5,6\text{-dimethyl-OP})_2Cu]^{2+}$ (5,6-dimethyl-OP = 5,6-dimethyl-1,10-

phenanthroline) induces a conformational transition from B to Z DNA. Inorg Chem 37:3927–3934
64. Satyanarayana S, Dabroniak JC, Chaires JB (1992) Neither.DELTA.-nor.LAMBDA.-tris(phenanthroline)ruthenium(II) binds to DNA by classical intercalation. Biochemistry 31:9319–9324
65. Satyanaryana S, Daborusak JC, Chaires JB (1993) Tris(phenanthroline)ruthenium(II) enantiomer interactions with DNA: mode and specificity of binding. Biochemistry 32:2573–2584
66. Liu Y, Chao H, Tan L, Yuan Y, Wei W, Ji L (2004) A comparative study of the interaction of two structurally analogue ruthenium(II) complexes with DNA. J Inorg Biochem 98:2011–2015
67. Onoa GB, Cervantes G, Moreno V, Prieto MJ (1998) Study of the interaction of DNA with cisplatin and other Pd(II) and Pt(II) complexes by atomic force microscopy. Nucleic Acids Res 26: 1473–1480